

Two-tone optomechanical instability in backaction-evading measurements

Itay Shomroni,^{1,*} Amir Youssefi,^{1,*} Nick Sauerwein,^{1,*} Liu Qiu,^{1,*} Paul Seidler,² Daniel Malz,³ Andreas Nunnenkamp,⁴ and Tobias J. Kippenberg^{1,†}

¹*Institute of Physics, École Polytechnique Fédérale de Lausanne, Lausanne 1015, Switzerland*

²*IBM Research Zurich, Säumerstrasse 4, Rüschlikon 8803, Switzerland*

³*Max-Planck-Institut für Quantenoptik, Hans-Kopfermann-Straße 1, 85741 Garching, Germany*

⁴*Cavendish Laboratory, University of Cambridge, Cambridge CB3 0HE, United Kingdom*

(Dated: June 9, 2022)

While quantum mechanics imposes a fundamental limit on the precision of interferometric measurements of mechanical motion due to measurement backaction, the nonlinear nature of the coupling also leads to parametric instabilities that place practical limits on the sensitivity by limiting the power in the interferometer. Such instabilities have been extensively studied in the context of gravitational wave detectors, and their presence has recently been reported in Advanced LIGO. Here we observe experimentally and describe theoretically a new type of optomechanical instability that arises in two-tone backaction-evading (BAE) measurements, designed to overcome the standard quantum limit (SQL), and demonstrate the effect in the optical domain with a photonic crystal nanobeam, and in the microwave domain with a micromechanical oscillator coupled to a microwave resonator. In contrast to the well-known oscillatory parametric instability that occurs in single-tone, blue-detuned pumping, which is characterized by a vanishing effective mechanical damping, the parametric instability in balanced two-tone optomechanics is exponential, and is a result of small detuning errors in the two pump frequencies. Its origin can be understood in a rotating frame as the vanishing of the effective mechanical frequency due to an optical spring effect. Counterintuitively, the instability occurs even in the presence of perfectly balanced intracavity fields, and can occur for both signs of detuning. We find excellent quantitative agreement with our theoretical predictions. Since the constraints on tuning accuracy become stricter with increasing probe power, it imposes a fundamental limitation on BAE measurements, as well as other two-tone schemes. In addition to introducing a new limitation in two-tone BAE measurements, the results also introduce a new type of nonlinear dynamics in cavity optomechanics.

I. INTRODUCTION

Interferometric position measurements of mechanical oscillators are the underlying principle of the Laser Interferometer Gravitational Observatory (LIGO) [1], and constitute one of the most sensitive absolute distance measurement techniques available to date. In a similar vein, cavity optomechanical systems [2], which exploit the radiation pressure coupling of light and mechanical motion in micro- and nanomechanical systems, have allowed to achieve some of the most sensitive measurements of mechanical motion relative to the zero-point motion [3, 4]. They can operate in a regime where measurement quantum backaction is relevant [5, 6], and where dynamical radiation pressure backaction cooling [7–9] and amplification is accessible [10–12]. In both settings, the quantum fluctuations of radiation pressure place a fundamental limitation on the displacement sensitivity [13, 14]. Yet, additionally, radiation pressure nonlinearities can equally pose a limit to sensitivity. Indeed, the oscillatory parametric instability [10–12, 15–19], is one of the most fundamental optomechanical effects predicted to limit the performance of the LIGO detector by constraining the optical power below the self-

induced oscillation threshold [10, 20–26]. It arises from the fact that the radiation-pressure coupling is intrinsically nonlinear, giving rise—in addition to static optical bi-stability [27]—to rich nonlinear dynamics, leading to an intricate landscape of multiple stable attractors (dynamical multi-stability) [12, 19, 28] and classical chaos [29]. Radiation-pressure induced parametric instability has been observed in cavity optomechanical systems [11], and a decade later in the Advanced LIGO detector itself [30]. It requires special measures to be taken for its suppression [31]. Understanding such dynamical instabilities in optomechanical systems is of importance for realizing ultra-sensitive displacement measurements that operate with high cooperativity. In addition, nonlinear phenomena in optomechanical systems have been the subject of experimental studies by themselves [28, 32, 33].

Here, we report a new type of instability that arises due to radiation pressure, distinct from the oscillatory parametric instability. The instability occurs in optomechanical systems driven with two tones, and it is of particular relevance to one class of quantum non-demolition (QND) measurements—two-tone backaction-evading (BAE) measurements, first proposed by Braginsky, Thorne, *et al.* [34–36]—that aim to surpass the standard quantum limit (SQL) of measurement of mechanical motion [36]. These BAE measurements proceed by pumping an optomechanical system (that resides in the resolved sideband limit [7]) simultaneously on the upper and lower motional sideband of the cavity, and al-

* These authors contributed equally.

† tobias.kippenberg@epfl.ch

low in principle arbitrary measurement sensitivity: by increasing the probing power, measurement imprecision is decreased, *without* incurring an additional measurement noise due to quantum backaction. Although theoretically proposed several decades ago, only advances in cavity optomechanics have allowed recently to enter the quantum backaction-dominated regime and to carry out BAE measurements in the microwave [37–40] and optical [41] domains. The here reported *two-tone instability* arises in the presence of finite-frequency detuning from the ideal BAE configuration, with respect to both optical and mechanical resonance frequencies. In contrast to the well-known oscillatory parametric instability that occurs in single-tone pumping on the upper motional sideband (or blue detuned in the bad cavity limit), which is characterized by a vanishing effective mechanical damping, the instability in balanced two-tone optomechanics can be understood in a rotating frame as the vanishing of the effective mechanical frequency due to an optical spring effect. We gain further insight by showing that the balanced two-tone scheme in the good-cavity (i.e. resolved sideband) limit can be mapped to single-tone optomechanics in the bad-cavity limit. Under these conditions, a qualitatively similar instability occurs as a result of bistability [2, 27, 42–44].

The allowed frequency deviation of the two probe tones to avoid instability decreases inversely with optical pump power. The two-tone instability thus imposes profound experimental requirements on its practical implementation, in the presence of ubiquitous experimental imperfections, or imperfect knowledge of the cavities' or mechanical oscillators' frequency. While we consider BAE it is important to note, that the reported effect can affect other two-tone optomechanical protocols, such as dissipative optomechanical squeezing of optical and microwave fields [45, 46] or mechanical motion [38, 39, 47–49]. We note that other BAE measurement instabilities have been reported before, and associated with parametric driving [51]. Early experiments [52] encountered such instabilities, attributed to dependence of the mechanical frequency on temperature [53] or two-level systems [54]. In contrast, the two-tone instability reported here arises purely from the optomechanical interaction and thus affects all optomechanical systems, depending *solely* on the achieved tuning accuracy. For any finite variation of pump frequency, a finite threshold exists and the two tone instability *fundamentally* limits the maximum probe power, and thus the achievable sensitivity.

II. OBSERVATION OF INSTABILITY IN TWO-TONE PUMPING

In a BAE measurement the cavity is probed with two pump tones, each tuned to the upper and lower motional sideband of the cavity, i.e., $\Delta_c = \pm\Omega_m$. It can mathematically also be understood as a single pump tuned to the cavity resonance ω_c exhibiting full (i.e., unity) extinc-

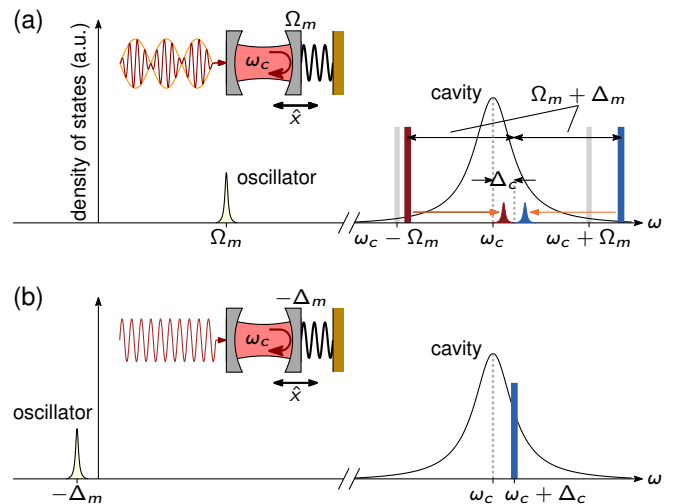


FIG. 1. **Pumping scheme leading to two-tone instability.** (a) Frequency-space representation of optical backaction evading (BAE) measurement using two-tone pumping. An optomechanical system is pumped with two pumps that are placed on the lower and upper motional sideband of the cavity (shown in grey). Two detuning errors are introduced, due to imperfect knowledge of the mechanical oscillator frequency (Δ_m), and due to imperfect symmetric spacing around the cavities' resonance frequency ω_c , as expressed by Δ_c . Also shown are the mechanical resonance at frequency Ω_m and the scattered mechanical sidebands. The inset shows an optomechanical system: a mechanical oscillator (position coordinate \hat{x}) that is the moving mirror of a Fabry-Perot cavity and that is coupled to the cavity mode by radiation pressure. (b) An equivalent system, in which the two-tone pumping is mapped to a Hamiltonian that exhibits the same dynamics as (a), which consists of a single continuous pump field applied at $\omega_c + \Delta_c$ and in which the mechanical oscillator frequency obeys the substitution $\Omega_m \rightarrow -\Delta_m$. Note that Δ_c and Δ_m have been exaggerated for clarity.

tion amplitude-modulation at the mechanical frequency Ω_m . In Fig. 1a we illustrate the scheme, and introduce a small detuning error $\Delta_c \ll \kappa$ of the symmetrically spaced tones with respect to the cavity resonance, as well as an error $\Delta_m \sim \Gamma_m$ in modulation frequency. As a result, the two tones are detuned by $\Delta_c \pm (\Omega_m + \Delta_m)$ from the cavity resonance. The motion of the oscillator, due to thermal noise from the environment and quantum backaction by the pump fields, is imprinted as fluctuations on the fields reflected from the optomechanical system. The corresponding output noise spectrum of the two probes exhibits two Lorentzians separated by $2\Delta_m$, also shown in Fig. 1a. When $\Delta_c = \Delta_m = 0$ an ideal BAE measurement is performed. The mechanical sidebands superimpose, but while thermal motion adds in quadrature, the quantum backaction noise, given in units of mechanical quanta by the optomechanical cooperativity \mathcal{C} , does not and is cancelled, leaving only thermal noise [37, 41, 55]. A hallmark of BAE measurements is to witness, as Δ_m is varied from a finite value to zero, a total mechanical noise that is lower than the weight of the two individual

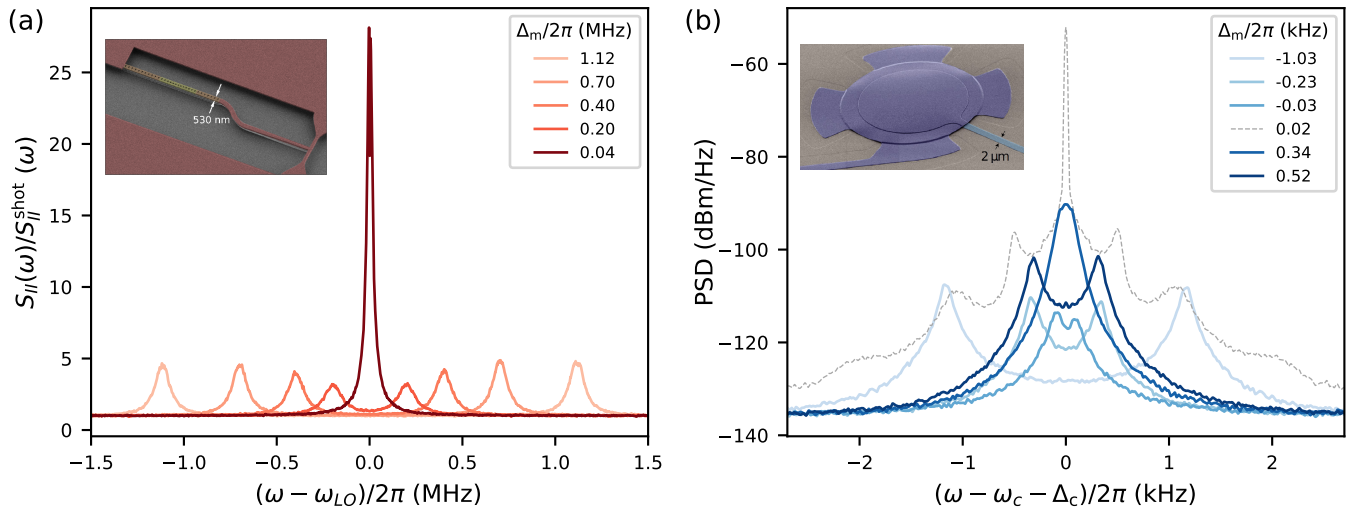


FIG. 2. **Experimental observation of two-tone instability.** (a) BAE measurement in the optical domain with an optomechanical system based on a silicon photonic crystal nanobeam (inset). A sequence of measurements is shown, where the mechanical sidebands are measured via quantum-limited heterodyne detection, here normalized to the shot-noise level. Here, ω_{LO} is the optical frequency of the heterodyne local oscillator laser. In the sequence, a mechanical ‘tuning error’ Δ_m is varied from positive to negative values, where $\Delta_m = 0$ ideally corresponding to a BAE measurement. Due to the cavity tuning error Δ_c , at $\Delta_m/2\pi = 0.04$ MHz a strong increase in the total mechanical noise is observed, as well as narrowing of the sideband, instead of the expected decrease due to backaction cancellation. This is the onset of the two-tone instability. (b) BAE measurement in the microwave domain with a mechanically-compliant capacitor coupled to a superconducting microwave resonator (inset). The procedure is the same as in (a). Measurements with both positive and negative values of Δ_m are shown. The measurement $\Delta_m/2\pi = 0.02$ kHz occurs within the domain of instability (grey dashed curve), and the spectrum is due to saturation of the HEMT amplifier, used in the detection chain. Note the logarithmic y -axis.

mechanical noise spectra.

Such BAE measurements have been carried out in the microwave domain in several experiments using mechanically-compliant capacitors [37–40], and have recently been extended to the optical domain [41]. We carried out BAE experiments using an optomechanical photonic crystal nanobeam operating at GHz frequencies embedded in a ^3He buffer gas cryostat, as detailed in prior work [41, 56]. The parameters of the devices are shown in Appendix C, and details of the measurement setup which uses a quantum-limited heterodyne detection are contained in Ref. 41. Figure 2a shows our BAE measurement in the optical domain. In this experiment the cooperativity was set to $\mathcal{C} \simeq 2.6$ and Δ_m scanned from positive to negative. However, instead of the expected decrease in total noise, indicating BAE, an exponential increase in the total noise is observed near $\Delta_m/2\pi = 40$ kHz. Upon further decrease in Δ_m , the system leaves the linear regime as the optical cavity undergoes self-oscillations, i.e., we observe an instability.

To independently confirm the existence and universality of this phenomenon, we performed the measurement in an entirely different optomechanical system: an electromechanical system based on mechanically-compliant vacuum-gap capacitor coupled to a superconducting microwave resonator embedded in a dilution refrigerator [57, 58]. Figure 2b shows this experiment, with a

cooperativity of $\mathcal{C} = 7$ (here, measurement backaction includes classical noise, which should also be cancelled). In this second measurement as well we observe an exponential increase in the total noise as the detuning Δ_m is decreased. As Δ_m is decreased further, the amplified noise saturates the HEMT amplifier in the detection chain leading to increased noise floor (Fig. 2a, grey dashed curve). In both experiments, BAE is not observed under the given experimental conditions.

The origin of this instability is not due to auxiliary effects in the experiments—as is expected based on the observation that the same behavior occurs in two very different optomechanical systems—and is, as shown below, a direct consequence of the optomechanical interaction, in the presence of the small tuning errors Δ_m and Δ_c , and depends only on these two parameters and the cooperativity. We next develop the theory behind this new instability in Sec. III, and perform a systematic experimental study in Sec. IV which fully confirms the theoretical predictions.

III. THEORY

It is well-known that the anti-damping induced by pumping the cavity on the upper motional sideband (or blue detuning in the bad cavity limit) can induce an os-

cillatory parametric instability. In principle, there exists another type of dynamical instability in this system, when the effective *mechanical frequency* vanishes, or in other words, when the restoring force disappears. This is known to occur in the bad-cavity regime for sufficiently strong driving with a red-detuned tone [2, 27, 42–44]. As the pump power increases, first a region of static bistability develops and eventually the original stable state becomes unstable. The departure from the stable state follows the same linearized equations and is also characterized by an exponential instability. This cannot occur in the resolved-sideband regime and when the mechanical frequency is large compared to the optomechanical coupling strength. Indeed, optomechanical systems typically employ high- Q oscillators where the shift in mechanical frequency due to dynamical backaction can be neglected. However, as we show below, this instability may arise when pumping with *two* tones, close to the upper and lower mechanical sidebands (Fig. 1a), as in BAE measurements, for example. In fact, as we will show, the two situations are described by the same linearized equations.

We model the system by the standard optomechanical Hamiltonian comprising one cavity mode with frequency ω_c , one mechanical mode with frequency Ω_m , and a nonlinear interaction $H_{\text{int}} = -\hbar g_0 \hat{a}^\dagger \hat{a} (\hat{b}^\dagger + \hat{b})$, where \hat{a} (\hat{b}) denote the optical (mechanical) annihilation operator. The cavity is driven by one or two coherent tones that produce a coherent intracavity field with amplitude $\bar{a}(t)$. We move to the interaction picture with respect to the Hamiltonian $\hat{H}_0 = \hbar \omega_l \hat{a}^\dagger \hat{a}$ and linearize the operators around their coherent amplitude $\hat{a} \rightarrow \bar{a}(t) + \delta \hat{a}$, $\hat{b} \rightarrow \bar{b} + \delta \hat{b}$. This yields the linearized Hamiltonian

$$\hat{H}/\hbar = -\Delta_c \delta \hat{a}^\dagger \delta \hat{a} + \Omega_m \delta \hat{b}^\dagger \delta \hat{b} - g(t) (\delta \hat{a} + \delta \hat{a}^\dagger) (\delta \hat{b} + \delta \hat{b}^\dagger) \quad (1)$$

where $g(t) = g_0 \bar{a}(t)$ denotes the field-enhanced coupling. We will consider two distinct situations: Single-tone driving on the upper motional sideband and balanced two-tone driving on upper and lower motional sideband. In single-tone driving, we have $\Delta_c = \Omega_m$ and $g(t) = g = \text{const.}$, whereas the two-tone driving is described through $\Delta_c \approx 0$ and $g(t) = g \cos[(\Omega_m + \Delta_m)t]$. Applying the rotating-wave approximation in two-tone driving but not in single-tone driving, both situations can be described by the same Hamiltonian

$$\hat{H}/\hbar = -\Delta_c \delta \hat{a}^\dagger \delta \hat{a} - \Delta_m \delta \hat{b}^\dagger \delta \hat{b} - g(\delta \hat{a} + \delta \hat{a}^\dagger) (\delta \hat{b} + \delta \hat{b}^\dagger), \quad (2)$$

where in single-tone driving, $\Delta_m = -\Omega_m$, whereas in two-tone driving, $\Delta_m \approx 0$. This equivalence is illustrated in Fig. 1b.

We describe the optomechanical system in terms of quantum Langevin equations [2, 59], which take into account decay into the cavity and mechanical bath. Eliminating the optical modes in frequency space, we arrive at an effective description for the mechanical mode only

$$\left[\frac{\Gamma_m}{2} - i(\Delta_m + \omega) + i\Sigma(\omega) \right] \delta \hat{b}(\omega) = -i\Sigma(\omega) \delta \hat{b}^\dagger(\omega) + \hat{\xi}_{\text{in}}(\omega), \quad (3)$$

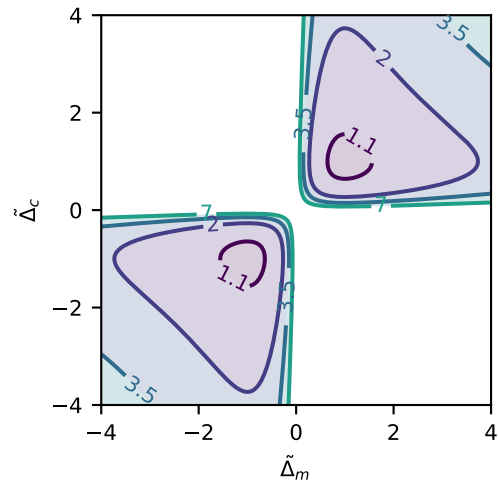


FIG. 3. **Domains of two-tone instability.** The onset of the two-tone instability is given by the condition (6) and depends only on $\tilde{\Delta}_m \equiv \Delta_m/(\Gamma_m/2)$, $\tilde{\Delta}_c \equiv \Delta_c/(\kappa/2)$, and the cooperativity \mathcal{C} . Here we plot the domains of instability as a function of $\tilde{\Delta}_m$ and $\tilde{\Delta}_c$ for different cooperativities \mathcal{C} (given as the contour labels). As \mathcal{C} increases the stable region in the vicinity of the origin $\tilde{\Delta}_m = \tilde{\Delta}_c = 0$ becomes smaller, reducing the range of $\tilde{\Delta}_m$ and $\tilde{\Delta}_c$ for which the system is stable.

where the self-energy (effective coupling) is given through

$$\Sigma(\omega) = \frac{2\Delta_c g^2}{(\kappa/2 - i\omega)^2 + \Delta_c^2}. \quad (4)$$

In Eq. (3) we have subsumed all noise contribution into a single generic noise input operator $\hat{\xi}_{\text{in}}(\omega)$, which does not play a role in the instability mechanism. So far we have not made any approximations (beyond the RWA in two-tone driving), and indeed Eq. (3) contains all the effects we wish to consider here. The self-energy Σ plays two roles. First, it couples $\delta \hat{b}^\dagger$ to $\delta \hat{b}$, thus acting like the coupling in a degenerate parametric oscillator. Second, as a self energy, its real part renormalizes the frequency of the mechanical resonator and its imaginary part modifies the effective damping.

Oscillatory instability.—In single-tone driving on the upper motional sideband, a parametric instability occurs if the optical anti-damping overcomes the intrinsic damping (i.e. $\mathcal{C} = 1$). In this regime, the right-hand side of Eq. (3) has hardly any effect, as the mechanical frequency is very large and it can be neglected in a RWA. The instability threshold can be extracted from the imaginary part of the effective susceptibility Eq. (4), $\text{Im}[\Sigma(\Omega_m)] \simeq \Gamma_m \mathcal{C}/2$, recovering the standard instability threshold ($\mathcal{C} = 1$), where the cooperativity is $\mathcal{C} = 4g^2/\kappa\Gamma_m$.

Exponential instability.—In backaction-evading measurements, however, Δ_m is small, as it represents a tuning error. This makes the right-hand side of Eq. (3) near resonant, such that it cannot be neglected. The instability arises in a way similar to a degenerate parametric oscil-

lator [60]. Since κ is now a large parameter, we can neglect the frequency dependence of $\Sigma(\omega) \approx \Sigma(0) \equiv \Sigma \in \mathbb{R}$, which allows us to recast Eq. (3) again as an equation of motion

$$\delta\dot{\hat{b}}(t) = \left[-\frac{\Gamma_m}{2} + i(\Delta_m - \Sigma) \right] \delta\hat{b}(t) - i\Sigma\delta\hat{b}^\dagger(t) + \hat{\xi}_{\text{in}}(t). \quad (5)$$

This equation is the same quantum Langevin equation as one would write down for a damped degenerate parametric oscillator. The dynamical matrix corresponding to Eq. (5) has eigenvalues $-\frac{\Gamma_m}{2} \pm \sqrt{\Delta_m(2\Sigma - \Delta_m)}$, yielding an instability threshold

$$4g^2\Delta_m\Delta_c = \left(\frac{\Gamma_m^2}{4} + \Delta_m^2 \right) \left(\frac{\kappa^2}{4} + \Delta_c^2 \right). \quad (6)$$

The instability threshold can also be written in terms of normalized detunings $\tilde{\Delta}_c \equiv \Delta_c/(\kappa/2)$ and $\tilde{\Delta}_m \equiv \Delta_m/(\Gamma_m/2)$ to read $4\mathcal{C} = (1 + \tilde{\Delta}_c^2)(1 + \tilde{\Delta}_m^2)/(\tilde{\Delta}_c\tilde{\Delta}_m)$. This equation can only be fulfilled for $\mathcal{C} \geq 1$, and we plot its contours in Fig. 3. In this instability, the effective frequency of the mechanical resonator vanishes, it ceases to oscillate and its amplitude simply grows exponentially, whereas in the previous case the instability was of an oscillatory kind, resulting from anti-damping. Note that Eq. (6) also predicts that the instability can occur for *both* negative and positive values of the two detuning errors, in contrast to the parametric instability.

IV. EXPERIMENT

To validate Eq. (6), the threshold for the two-tone instability in terms of Δ_m, Δ_c , we perform a two-dimensional scan in the clean and well-controlled setting of circuit electromechanics, in a system based on mechanically-compliant vacuum-gap capacitor coupled to a superconducting resonant circuit, embedded in a dilution refrigerator [57, 58]. Here, pump frequency fluctuations and cavity frequency fluctuations are significantly smaller than in the optical domain, and the detuning can be accurately controlled. Full detail on the system and experiment are given in Appendix B. We present measurements in the optical domain in Appendix C.

Figure 4a–c shows the total noise in the mechanical sidebands as a function of $\tilde{\Delta}_m$ and $\tilde{\Delta}_c$ for three different cooperativities \mathcal{C} . Each horizontal cut in Fig. 4a–c corresponds to a measurement of the type shown in Fig. 2a. The domains of instability are clearly evident as areas of increased noise (in red), in excellent agreement with Eq. (6) (black contours). In particular, instability only arises when $\tilde{\Delta}_m\tilde{\Delta}_c > 0$ as predicted from Eq. (6), and can arise both for red- ($\tilde{\Delta}_c < 0$) and blue-detuned ($\tilde{\Delta}_c > 0$) mean probe frequency. Figure 4d–f shows the theoretical plots corresponding to Fig. 4a–c, again in excellent agreement. Figure 4g–i shows the horizontal cuts indicated in Fig. 4b. The point $\tilde{\Delta}_m = \tilde{\Delta}_c = 0$ corresponds to a ‘perfect’ BAE measurement, as can be seen in Fig. 4g where

a 3 dB decrease in the total mechanical noise relative to $\tilde{\Delta}_m \neq 0$ is evident, due to cancellation of measurement backaction.

In Appendix B we show experimentally that at the onset of instability, the effective mechanical frequency (due to the optical spring) equals the pump modulation frequency (i.e. the effective mechanical frequency vanishes in the rotating frame). In other words, while the instability occurs for $\Delta_m \neq 0$, in the experiment the sidebands coincide at the onset of instability.

Figure 4 demonstrates experimentally the decrease in size of the stable region with increasing pumping power, with $\tilde{\Delta}_c \lesssim 1/2\mathcal{C}$ required to avoid instability (e.g., $\tilde{\Delta}_c \lesssim 0.04$ for $\mathcal{C} = 14$ in Fig. 4c). Overall excellent agreement is obtained between theory and experiment, confirming our theoretical analysis and description of the effect. Thus optomechanics imposes strict tuning accuracy for a given measurement sensitivity in two-tone BAE measurements. In this case, measurement backaction is due to both quantum and classical noise in the two microwave tones. It is important to emphasize that for BAE measurements that allow measurements beyond the SQL, cooperativities of $\mathcal{C} \gg \bar{n}_m$ are required, thus highlighting the stringent nature of the condition imposed by $\tilde{\Delta}_c \lesssim 1/2\mathcal{C}$.

V. CONCLUSION

We reported experimentally and explained theoretically a new type on dynamical instability that was previously unobserved (and inaccessible) in cavity optomechanics. This instability is qualitatively different from the oscillatory parametric instability [10, 12, 17–20, 61], and has its origin not in the vanishing of the imaginary parts of the effective mechanical susceptibility, but that of the real part (i.e. the mechanical oscillator frequency). Apart from expanding the landscape of nonlinear phenomena in optomechanics, our work entails that, as optomechanics in the optical domain advance toward more complicated experiments involving multiple tone driving [41, 45, 47, 62, 63], the performance will be subject to stricter demands on pump tuning accuracy and stability.

ACKNOWLEDGMENTS

This work was supported by funding from the Swiss National Science Foundation under grant agreement No. NCCR-QSIT: 51NF40-160591. The microwave sample was fabricated in the Center of MicroNanoTechnology (CMi) at EPFL. The photonic sample was fabricated at IBM Research, Zurich. DM acknowledges support by the ERC Advanced Grant QUENOCOBA under the EU Horizon 2020 program (grant agreement 742102). AN acknowledges a University Research Fellowship from the Royal Society and support from the Winton Programme for the Physics of Sustainability. This work

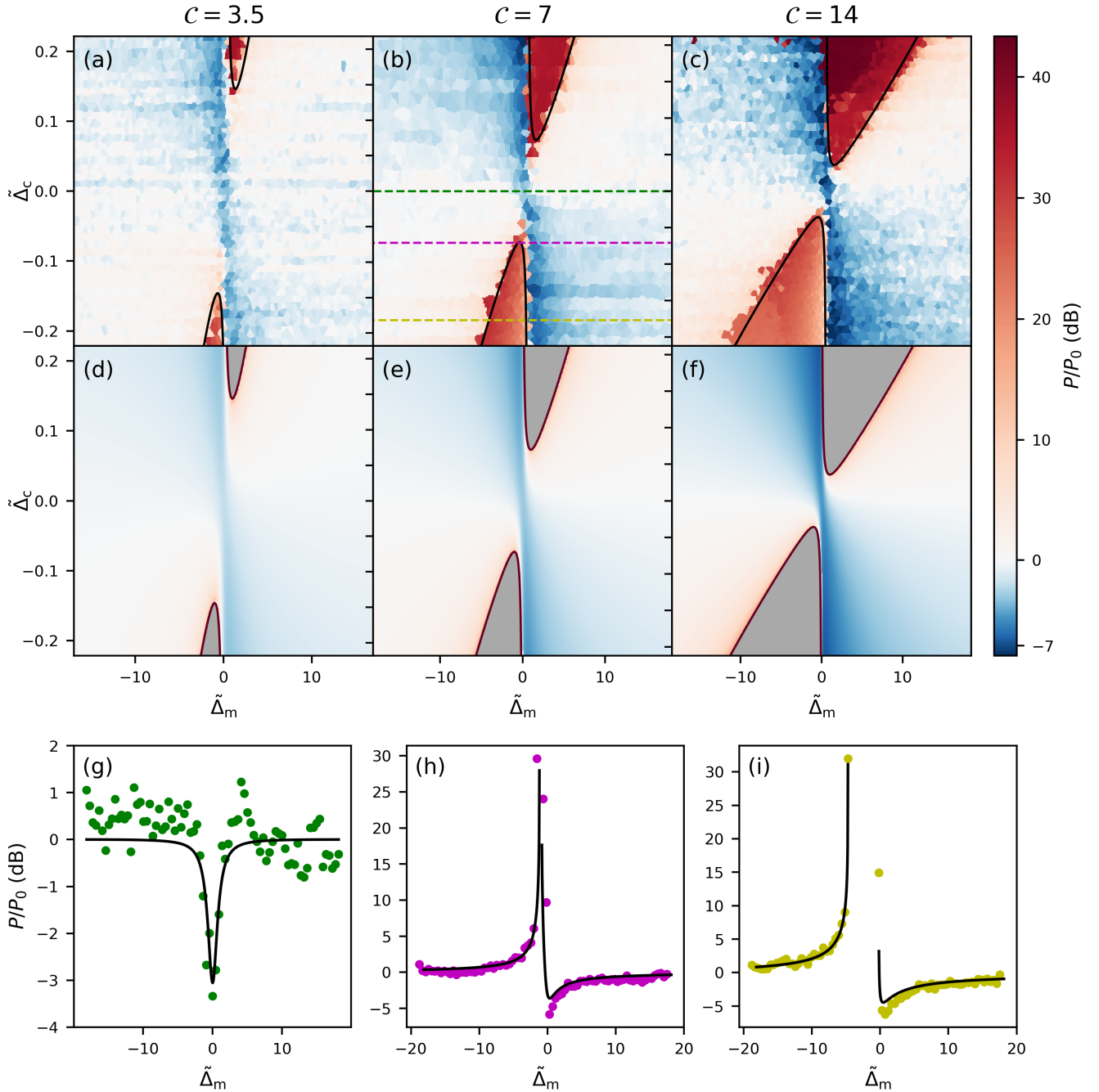


FIG. 4. **Investigation of the two-tone instability in a circuit-electromechanical system.** (a–c) Mapping of the total mechanical noise as a function of $\tilde{\Delta}_m$ and $\tilde{\Delta}_c$, for cooperativities $\mathcal{C} = \{3.5, 7, 14\}$ respectively. The total power P in both mechanical sidebands in the output spectra is shown, normalized to the power P_0 at $(\tilde{\Delta}_m, \tilde{\Delta}_c) = (-18, 0)$ (no tuning error and far from BAE regime). Since data points do not align on a regular grid (accounting for small changes in $\tilde{\Delta}_c$ along the horizontal scan), the rasterization was implemented using nearest-neighbor (Voronoi) partitioning. Solid black lines are instability thresholds from Eq. (6). (d–f) Theory plots corresponding to (a–c). Gray areas are theory predicted unstable regions. (g–i) Cross-sections of (b) for $\tilde{\Delta}_c = \{0, -0.07, -0.18\}$ respectively [nearest data points to horizontal dashed lines in (b)]. Solid black lines are theory predictions based on the full linear model.

was supported by the European Union's Horizon 2020 research and innovation programme under grant agreement No. 732894 (FET Proactive HOT).

Appendix A: Eigenvalues of the dynamical matrix

Further understanding of the two-tone instability, and its distinction from the parametric instability, can be achieved by examining the eigenvalues of the dynamical matrix, similar to the analysis performed in [50]. The Hamiltonian (2) leads to the quantum Langevin equations

$$\delta \dot{\hat{a}} = -(\kappa/2 - i\Delta_c)\delta \hat{a} + ig(\delta \hat{b} + \delta \hat{b}^\dagger) + \sqrt{\kappa}\delta \hat{a}_{\text{in}} \quad (\text{A1a})$$

$$\delta \dot{\hat{b}} = -(\Gamma_m/2 - i\Delta_m)\delta \hat{b} + ig(\delta \hat{a} + \delta \hat{a}^\dagger) + \sqrt{\Gamma_m}\delta \hat{b}_{\text{in}}. \quad (\text{A1b})$$

Ignoring the input noise operators $\delta \hat{a}_{\text{in}}$ and $\delta \hat{b}_{\text{in}}$ which are irrelevant in the present analysis, the Langevin Eqs. (A1) can be written as a matrix equation $\dot{\mathbf{x}} = \mathbf{M}\mathbf{x}$ with

$$\mathbf{M} = \begin{pmatrix} -\kappa/2 & -\Delta_c & 0 & 0 \\ \Delta_c & -\kappa/2 & 2g & 0 \\ 0 & 0 & -\Gamma_m/2 & -\Delta_m \\ 2g & 0 & \Delta_m & -\Gamma_m/2 \end{pmatrix} \quad (\text{A2})$$

and

$$\mathbf{x} = [\delta \hat{a} + \delta \hat{a}^\dagger, i(\delta \hat{a}^\dagger - \delta \hat{a}), \delta \hat{b} + \delta \hat{b}^\dagger, i(\delta \hat{b}^\dagger - \delta \hat{b})]^T. \quad (\text{A3})$$

We recall that this dynamical equation describes *both* single-tone pumping, with the equivalence $-\Delta_m \rightarrow \Omega_m$, and two-tone pumping in the well-resolved sideband regime (Fig. 1). An eigenvalue of the matrix (A2) with a positive real part leads to an exponentially increasing solution, and thus signals an instability.

Figure 5 shows the domains of instability in the parameter space spanned by Δ_m and Δ_c . These domains separate into two classes, corresponding to the parametric and two-tone instabilities. In one class, which corresponds to the conventional parametric instability, the imaginary part of the offending eigenvalue is nonzero, thus the instability is of an *oscillatory* character.

This class lies in the vicinity of the diagonal $\Delta_c \approx \Omega_m$, as expected (note that the regime $\Delta_m = -\Omega_m > 0$ although mathematically possible, is unphysical in this case). The second class lies close to the origin, in particular $|\Delta_m| \ll \kappa$, and corresponds to the two-tone instability. Here the imaginary part of the eigenvalue is zero, and the system does not oscillate, thus the instability is of an *exponential* character, as expected from vanishing of the mechanical frequency (in the rotating frame) in our analysis in Sec. III. These two-tone instability domains are also shown in Fig. 3 and are given by the simple condition (6).

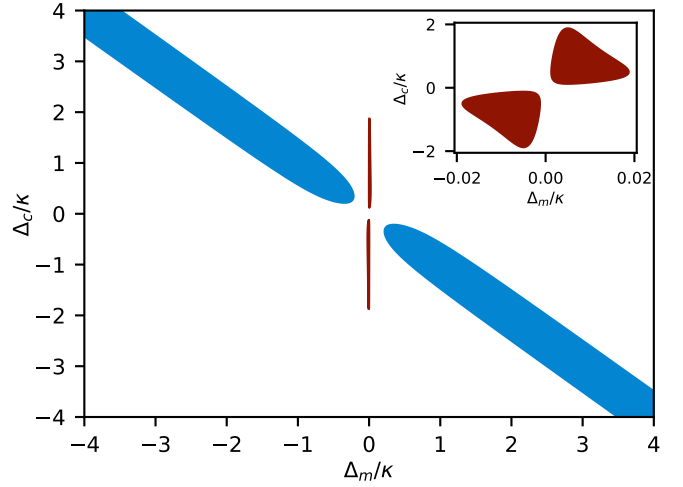


FIG. 5. **Instability domains from eigenvalue analysis.** Domains where an eigenvalue of the dynamical matrix (A2) has positive real part, signalling an instability. The blue domain, in the neighborhood of $-\Delta_m = \Omega_m \approx \Delta_c$ is the known parametric instability. In this domain, the imaginary part of the eigenvalue is nonzero (oscillatory instability). In reality, the mechanical frequency is positive $\Omega_m > 0$, such that the lower right part is unphysical. The red domain that occurs for $|\Delta_m| \ll \kappa$ (zoom shown in the inset) is the two-tone instability. In this domain $\Delta_m\Delta_c > 0$, and the imaginary part of the eigenvalue is zero (exponential instability). The parameters used are $\kappa = 1$, $\Gamma_m = 10^{-2}$, and $\mathcal{C} = 2$.

Appendix B: Microwave experiment details

For the microwave-domain part of this work, we used a system similar to the one described in Ref. 58. Specifically, an overcoupled ($\kappa_{\text{ex}}/2\pi = 2.65$ MHz, $\kappa_0/2\pi = 0.16$ MHz) Al superconducting microwave resonator with a resonance frequency of $\omega_c/2\pi = 6.43$ GHz that was coupled (vacuum coupling rate $g_0/2\pi = 194$ Hz) to a mechanically-compliant vacuum gap capacitor ($\Omega_m/2\pi = 6.15$ MHz and $\Gamma_m/2\pi \approx 20$ Hz). The chip was cooled to about 15 mK in a dilution refrigerator.

In the experiment, we used three microwave sources with a common frequency reference to pump the optomechanical system: two BAE pumps with frequencies $\omega_c + \Delta \pm (\Omega_m + \Delta_m)$, and an additional cooling pump tuned to $\omega_c - \Omega_m - \delta_{\text{cool}}$, where $\delta_{\text{cool}}/2\pi = 400$ kHz. The purpose of the cooling pump was to reduce the thermal occupation of the mechanical oscillator, thereby reducing the fluctuations in power of the mechanical sidebands that originate from fluctuations of the base temperature and vibrations of the dilution refrigerator, since the oscillator is dominantly coupled to the microwave bath. The cooling tone also increased the mechanical damping rate to $\Gamma_{\text{eff}}/2\pi = 110$ Hz, allowing us to observe the narrowing of the mechanical sidebands when approaching the instability with better resolution.

To take the data in Fig. 4, we first measured the cavity resonance frequency ω_c by applying the cooling tone

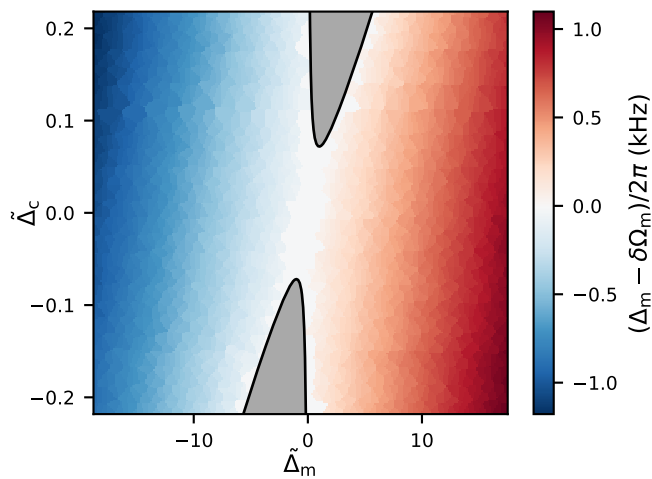


FIG. 6. **Vanishing of the effective mechanical frequency.** The plot shows the difference between the measured effective mechanical frequency and pump modulation frequency as a function of the detunings. Near the instability domain (shaded in gray), the two frequencies become equal, which corresponds to vanishing of the effective mechanical frequency in the rotating frame, confirming the theoretical treatment. Measurement is the same as in Fig. 4b.

alone and acquiring the microwave response [64]. We then placed the BAE pumps symmetrically around the resonance, $\Delta_c = 0$, and measured the mechanical resonance frequency Ω_m using the distance between the peaks of the mechanical sidebands. The data of Fig. 4 were taken along horizontal scans, by first setting the required Δ_c and varying Δ_m , acquiring noise spectra as in Fig. 2b. Prior to taking each horizontal line, we followed a procedure to ensure that no additional mechanical loss or amplification was introduced by the BAE pumps that might lead to parametric instability: First, only the red BAE pump was applied and its power optimized such that the width of mechanical sideband corresponds to the desired single tone cooperativity \mathcal{C} (computed from the additional damping introduced). Second, the blue BAE pump was added, and its power adjusted such that the width of the mechanical sideband narrows back to Γ_{eff} . This procedure was also followed prior to measurement of Ω_m .

To account for cavity frequency fluctuations, the microwave frequency ω_c was also measured after each single point (Δ_m, Δ_c) . This results in a slight vertical scatter along the horizontal scan. We used nearest-neighbor (Voronoi) partitioning, to present the full two-dimensional image. In addition, we disconnected all pumps for two seconds, between data points, to let the mechanical oscillator thermalize and cancel any hysteresis effects due to the instability.

In Fig. 6 we plot the difference between Δ_m and the change in effective mechanical frequency of the oscillator $\delta\Omega_m$ (due to the optical spring effect), for the same data as in Fig. 4b. Near the onset of the two-tone in-

stability, the two sidebands coincide, and this difference approaches zero, i.e., the effective mechanical frequency $\Omega_m + \delta\Omega_m$ becomes equal to the modulation frequency of the pump, $\Omega_m + \Delta_m$. This corresponds to vanishing of the effective mechanical frequency in the frame rotating with the modulation frequency. This confirms the exponential character of the two-tone instability, as predicted theoretically in Sec. III.

Appendix C: Observation of two-tone instability in the optical domain

As shown in Fig. 2a, we also observed the two-tone instability in an optomechanical system operating in the optical domain. The system is an optomechanical photonic crystal nanobeam [8, 65] with a mechanical frequency $\Omega_m/2\pi \simeq 5.2$ GHz, optical resonance frequency $\omega_c \simeq 194$ THz (wavelength $\lambda \simeq 1540$ nm), and cavity linewidth $\kappa/2\pi = 300$ MHz (optical Q factor $\sim 6.5 \times 10^5$). The vacuum optomechanical coupling rate is $g_0/2\pi = 930$ kHz. The sample is embedded in a ^3He buffer gas cryostat (Oxford Instruments HelioxTL), as reported previously [41, 56]. The buffer gas facilitates the thermalization of the sample, preventing prohibitive optical absorption heating and allows strong pumping. The controlled pressure of the buffer gas affects the damping rate of the oscillator. The different measurements reported here were done at temperatures in the range 4.6–4.9 K, and pressures 32–160 mbar, resulting in damping rate $\Gamma_m/2\pi = 100$ –285 kHz.

Figure 7 shows examples of the BAE measurements introduced in Sec. II, with Δ_m scanned from positive to negative values, while holding Δ_c approximately constant. Two measurements of similar cooperativities $\mathcal{C} \sim 2.2$ –2.6 are shown in Fig. 7a. In the lower measurement Δ_c is farther from 0, bringing it in the vicinity of the domain of instability (see Fig. 3), which is triggered on the next data point (not shown). This is the same measurement as Fig. 2a. The separation between data and domain of instability is $\sim 2\pi \times 15$ MHz, well within the uncertainty in our measurement of Δ_c . Figure 7b shows similar data for higher cooperativity $\mathcal{C} \sim 4$, where uncertainty in measurement of Δ_c precludes discerning between the stable and unstable behavior. Figure 7c shows the total mechanical noise in the data of Fig. 7a, with theoretical fit obtained from the Langevin Eqs. (A1). The data shown in light red, not encountering the instability, shows imperfect, asymmetric BAE behavior (due to $\Delta_c \neq 0$). The dark red data show the amplified noise prior to the onset of instability.

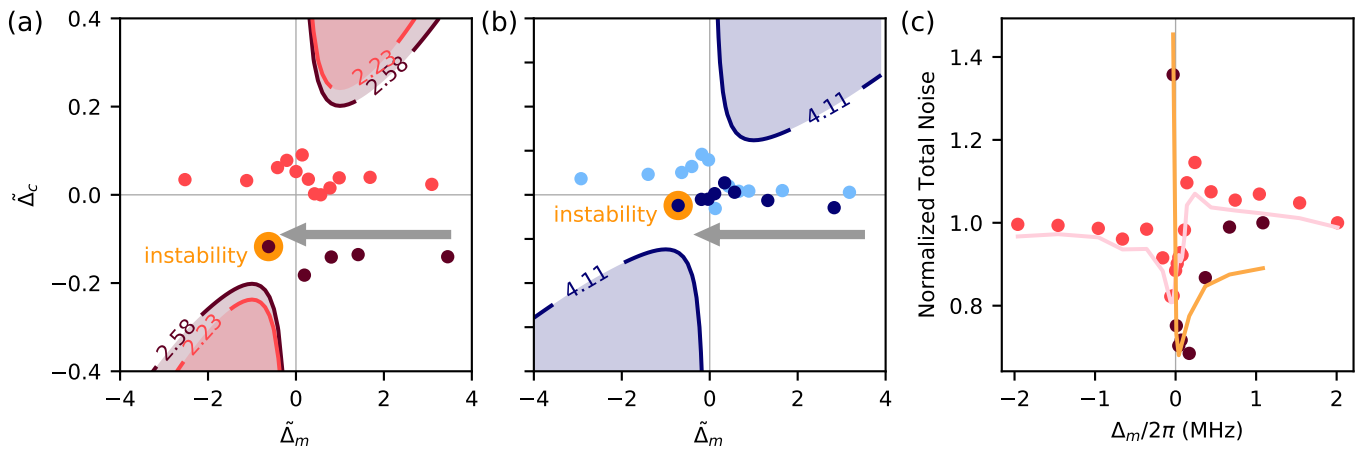


FIG. 7. **Two-tone instability in the optical domain.** (a) Two-tone BAE measurements (dark- and light-red dots) scanning Δ_m with Δ_c kept approximately constant. The $(\tilde{\Delta}_m, \tilde{\Delta}_c)$ coordinate of each measurement is plotted. The instability contours for the respective cooperativities, around $\mathcal{C} \sim 2.2$ – 2.6 (contour label), are indicated with the same color. While the upper measurement sequence remains near $\tilde{\Delta}_c \approx 0$, the lower sequence hits instability in the vicinity of the expected domain. The highlighted dot is the measurement right before instability. (b) Same as (a) with higher $\mathcal{C} \sim 4.1$. Here the stable region is smaller, highlighting the difficulty of achieving stable operation due to the inaccuracy in $\tilde{\Delta}_c$. (c) Total noise power in the mechanical sidebands, normalized to 1 for large Δ_m , for the two measurements sequences in (a). The sudden increase in power for the unstable data is seen. The solid lines are theoretical fits using the full Langevin equations. See text for more details.

- [1] LIGO Scientific Collaboration and Virgo Collaboration, *Physical Review Letters* **116**, 061102 (2016).
- [2] M. Aspelmeyer, T. J. Kippenberg, and F. Marquardt, *Reviews of Modern Physics* **86**, 1391 (2014).
- [3] D. J. Wilson, V. Sudhir, N. Piro, R. Schilling, A. Ghadimi, and T. J. Kippenberg, *Nature* **524**, 325 (2015).
- [4] M. Rossi, D. Mason, J. Chen, Y. Tsaturyan, and A. Schliesser, *Nature* **563**, 53 (2018).
- [5] T. P. Purdy, R. W. Peterson, and C. A. Regal, *Science* **339**, 801 (2013).
- [6] J. Teufel, F. Lecocq, and R. Simmonds, *Physical Review Letters* **116**, 013602 (2016).
- [7] A. Schliesser, R. Rivière, G. Anetsberger, O. Arcizet, and T. J. Kippenberg, *Nature Physics* **4**, 415 (2008).
- [8] J. Chan, T. P. M. Alegre, A. H. Safavi-Naeini, J. T. Hill, A. Krause, S. Gröblacher, M. Aspelmeyer, and O. Painter, *Nature* **478**, 89 (2011).
- [9] J. D. Teufel, T. Donner, D. Li, J. W. Harlow, M. S. Allman, K. Cicak, A. J. Sirois, J. D. Whittaker, K. W. Lehnert, and R. W. Simmonds, *Nature* **475**, 359 (2011).
- [10] V. B. Braginsky, S. E. Strigin, and S. P. Vyatchanin, *Physics Letters A* **287**, 331 (2001).
- [11] T. J. Kippenberg, H. Rokhsari, T. Carmon, A. Scherer, and K. J. Vahala, *Physical Review Letters* **95**, 033901 (2005).
- [12] F. Marquardt, J. G. E. Harris, and S. M. Girvin, *Physical Review Letters* **96**, 103901 (2006).
- [13] C. M. Caves, *Physical Review Letters* **45**, 75 (1980).
- [14] A. F. Pace, M. J. Collett, and D. F. Walls, *Physical Review A* **47**, 3173 (1993).
- [15] V. B. Braginsky and A. B. Manukin, *JETP* **25**, 653 (1967).
- [16] V. B. Braginsky and A. B. Manukin, *Measurement of weak forces in physics experiments* (University of Chicago Press, Chicago, 1977).
- [17] J. M. Aguirregabiria and L. Bel, *Physical Review A* **36**, 3768 (1987).
- [18] L. Bel, J.-L. Boulanger, and N. Deruelle, *Physical Review A* **37**, 1563 (1988).
- [19] M. Ludwig, B. Kubala, and F. Marquardt, *New Journal of Physics* **10**, 095013 (2008).
- [20] A. Pai, S. V. Dhurandhar, P. Hello, and J.-Y. Vinet, *The European Physical Journal D* **8**, 333 (2000).
- [21] V. B. Braginsky, S. E. Strigin, and S. P. Vyatchanin, *Physics Letters A* **305**, 111 (2002).
- [22] S. W. Schemm, C. Zhao, L. Ju, and D. G. Blair, *Classical and Quantum Gravity* **21**, S1253 (2004).
- [23] L. Ju, S. Grass, C. Zhao, J. Degallaix, and D. G. Blair, *Journal of Physics: Conference Series* **32**, 282 (2006).
- [24] L. Ju, S. Gras, C. Zhao, J. Degallaix, and D. G. Blair, *Physics Letters A* **354**, 360 (2006).
- [25] L. Ju, C. Zhao, S. Gras, J. Degallaix, D. G. Blair, J. Munch, and D. H. Reitze, *Physics Letters A* **355**, 419 (2006).
- [26] A. G. Gurkovsky, S. E. Strigin, and S. P. Vyatchanin, *Physics Letters A* **362**, 91 (2007).
- [27] A. Dorsel, J. D. McCullen, P. Meystre, E. Vignes, and H. Walther, *Physical Review Letters* **51**, 1550 (1983).
- [28] A. G. Krause, J. T. Hill, M. Ludwig, A. H. Safavi-Naeini, J. Chan, F. Marquardt, and O. Painter, *Physical Review Letters* **115**, 233601 (2015).
- [29] L. Bakemeier, A. Alvermann, and H. Fehske, *Physical Review Letters* **114**, 013601 (2015).
- [30] M. Evans, S. Gras, P. Fritschel, J. Miller, L. Barsotti, D. Martynov, A. Brooks, D. Coyne, R. Abbott, R. X. Adhikari, K. Arai, R. Bork, B. Kells, J. Rollins, N. Smith-Lefebvre, G. Vajente, H. Yamamoto, C. Adams, S. Aston, J. Betzweiser, V. Frolov, A. Mullavey, A. Pele, J. Romie, M. Thomas, K. Thorne, S. Dwyer, K. Izumi, K. Kawabe, D. Sigg, R. Derosa, A. Effler, K. Kokeyama, S. Ballmer, T. J. Massinger, A. Staley, M. Heinze, C. Mueller, H. Grote, R. Ward, E. King, D. Blair, L. Ju, and C. Zhao, *Physical Review Letters* **114**, 161102 (2015).
- [31] J. Miller, M. Evans, L. Barsotti, P. Fritschel, M. MacInnis, R. Mittleman, B. Shapiro, J. Soto, and C. Torrie, *Physics Letters A* **375**, 788 (2011).
- [32] F. Monifi, J. Zhang, c. K. Özdemir, B. Peng, Y.-x. Liu, F. Bo, F. Nori, and L. Yang, *Nature Photonics* **10**, 399 (2016).
- [33] D. Navarro-Urrios, N. E. Capuj, M. F. Colombano, P. D. García, M. Sledzinska, F. Alzina, A. Griol, A. Martínez, and C. M. Sotomayor-Torres, *Nature Communications* **8**, 14965 (2017).
- [34] K. S. Thorne, R. W. P. Drever, C. M. Caves, M. Zimmermann, and V. D. Sandberg, *Physical Review Letters* **40**, 667 (1978).
- [35] V. B. Braginsky, Y. I. Vorontsov, and K. S. Thorne, *Science* **209**, 547 (1980).
- [36] C. M. Caves, K. S. Thorne, R. W. P. Drever, V. D. Sandberg, and M. Zimmermann, *Reviews of Modern Physics* **52**, 341 (1980).
- [37] J. Suh, A. J. Weinstein, C. U. Lei, E. E. Wollman, S. K. Steinke, P. Meystre, A. A. Clerk, and K. C. Schwab, *Science* **344**, 1262 (2014).
- [38] F. Lecocq, J. Clark, R. Simmonds, J. Aumentado, and J. Teufel, *Physical Review X* **5**, 041037 (2015).
- [39] C. Lei, A. Weinstein, J. Suh, E. Wollman, A. Kronwald, F. Marquardt, A. Clerk, and K. Schwab, *Physical Review Letters* **117**, 100801 (2016).
- [40] C. Ockeloen-Korppi, E. Damskägg, J.-M. Pirkkalainen, A. Clerk, M. Woolley, and M. Sillanpää, *Physical Review Letters* **117**, 140401 (2016).
- [41] I. Shomroni, L. Qiu, D. Malz, A. Nunnenkamp, and T. J. Kippenberg, *arXiv:1809.01007* (2018).
- [42] P. Meystre, E. M. Wright, J. D. McCullen, and E. Vignes, *J. Opt. Soc. Am. B* **2**, 1830 (1985).
- [43] A. Gozzini, I. Longo, S. Barbarino, F. Maccarrone, and F. Mango, *Journal of the Optical Society of America B* **2**, 1841 (1985).
- [44] S. Aldana, C. Bruder, and A. Nunnenkamp, *Physical Review A* **88**, 043826 (2013), 1306.0415.
- [45] A. Kronwald, F. Marquardt, and A. A. Clerk, *New Journal of Physics* **16**, 063058 (2014).
- [46] C. Ockeloen-Korppi, E. Damskägg, J.-M. Pirkkalainen, T. Heikkilä, F. Massel, and M. Sillanpää, *Physical Review Letters* **118**, 103601 (2017).
- [47] A. Kronwald, F. Marquardt, and A. A. Clerk, *Physical Review A* **88**, 063833 (2013).
- [48] E. E. Wollman, C. U. Lei, A. J. Weinstein, J. Suh, A. Kronwald, F. Marquardt, A. A. Clerk, and K. C. Schwab, *Science* **349**, 952 (2015).

- [49] J.-M. Pirkkalainen, E. Damskäg, M. Brandt, F. Massel, and M. Sillanpää, *Physical Review Letters* **115**, 243601 (2015).
- [50] D. Malz and A. Nunnenkamp, *Physical Review A* **94**, 023803 (2016).
- [51] S. K. Steinke, K. C. Schwab, and P. Meystre, *Physical Review A* **88**, 023838 (2013).
- [52] J. B. Hertzberg, T. Rocheleau, T. Ndukum, M. Savva, A. A. Clerk, and K. C. Schwab, *Nature Physics* **6**, 213 (2010).
- [53] J. Suh, M. D. Shaw, H. G. LeDuc, A. J. Weinstein, and K. C. Schwab, *Nano Letters* **12**, 6260 (2012).
- [54] J. Suh, A. J. Weinstein, and K. C. Schwab, *Applied Physics Letters* **103**, 052604 (2013).
- [55] A. A. Clerk, F. Marquardt, and K. Jacobs, *New Journal of Physics* **10**, 095010 (2008).
- [56] L. Qiu, I. Shomroni, M. A. Ioannou, D. Malz, A. Nunnenkamp, and T. J. Kippenberg, [arXiv:1805.12364](https://arxiv.org/abs/1805.12364) (2018).
- [57] L. D. Tóth, N. R. Bernier, A. Nunnenkamp, A. K. Feofanov, and T. J. Kippenberg, *Nature Physics* **13**, 787 (2017).
- [58] N. R. Bernier, L. D. Tóth, A. Koottandavida, M. A. Ioannou, D. Malz, A. Nunnenkamp, A. K. Feofanov, and T. J. Kippenberg, *Nature Communications* **8**, 604 (2017).
- [59] C. W. Gardiner and P. Zoller, *Quantum noise*, 3rd ed. (Springer, 2004).
- [60] D. Walls and G. J. Milburn, *Quantum Optics*, edited by D. Walls and G. J. Milburn (Springer Berlin Heidelberg, Berlin, Heidelberg, 2008).
- [61] C. Fabre, M. Pinard, S. Bourzeix, A. Heidmann, E. Giacobino, and S. Reynaud, *Physical Review A* **49**, 1337 (1994).
- [62] M. J. Woolley and A. A. Clerk, *Physical Review A* **87**, 063846 (2013).
- [63] M. J. Woolley and A. A. Clerk, *Physical Review A* **89**, 063805 (2014).
- [64] N. R. Bernier, *Multimode microwave circuit optomechanics as a platform to study coupled quantum harmonic oscillators*, doctoral dissertation, EPFL (2018), section 3.5.1.
- [65] M. Eichenfield, J. Chan, R. M. Camacho, K. J. Vahala, and O. Painter, *Nature* **462**, 78 (2009).